CHINESE OPTICS LETTERS

Vol. 22, No. 2 | February 2024

Flexible one-dimensional photonic crystal films composed of chalcogenide glass and water-soluble polymer for curvature sensing

Xinyu Chen (陈新宇)[1,†], Zhangcheng Li (黎张成)[1,†], Ruolan Zhao (赵若兰)[1,†], Yu He (何 钰)[1], Yue He (何 月)[1], Zhi Liang (梁 治)[1], Guangming Tao (陶光明)[2,3,4], and Chong Hou (侯 冲)[1,2,5*]

[1] School of Optical and Electronic Information, Huazhong University of Science and Technology, Wuhan 430074, China

[2] Wuhan National Laboratory for Optoelectronics, Huazhong University of Science and Technology, Wuhan 430074, China

[3] Key Laboratory of Vascular Aging, Ministry of Education, Tongji Hospital Tongji Medical College, Huazhong University of Science and Technology, Wuhan 430030, China

[4] State Key Laboratory of Material Processing and Die & Mould Technology, School of Materials Science and Engineering, Huazhong University of Science and Technology, Wuhan 430074, China

[5] Shenzhen Huazhong University of Science and Technology Research Institute, Shenzhen 518063, China

[†] These authors contributed equally to this work.

*Corresponding author: chong@hust.edu.cn

Received August 7, 2023 | Accepted August 22, 2023 | Posted Online February 29, 2024

Curvature sensing plays an important role in structural health monitoring, damage detection, real-time shape control, modification, etc. Developing curvature sensors with large measurement ranges, high sensitivity, and linearity remains a major challenge. In this study, a curvature sensor based on flexible one-dimensional photonic crystal (1D-PC) films was proposed. The flexible 1D-PC films composed of dense chalcogenide glass and water-soluble polymer materials were fabricated by solution processing. The flexible 1D-PC film curvature sensor has a wide measurement range of 33–133 m^{-1} and a maximum sensitivity of 0.26 nm/m^{-1}. The shift of the transmission peak varies approximately linearly with the curvature in the entire measurement range. This kind of 1D-PC film curvature sensor provides a new idea for curvature sensing and measurement.

Keywords: curvature sensor; one-dimensional photonic crystals; solution processing; chalcogenide glass; flexible film.
DOI: 10.3788/COL202422.021601

1. Introduction

Curvature sensing plays an important role in mechanical bending angle measurement, human posture detection, bridge and road construction, structural deformation, and other mechanical engineering and structural health monitoring fields[1–4]. Compared with electrical curvature sensors, the optical curvature sensor has the advantages of small size, anti-electromagnetic interference, corrosion resistance, high sensitivity, and low maintenance cost, so it has been widely used in bending measurement[5]. Common optical curvature sensors include curvature sensing fiber and other technologies[6–9]. But there are still some problems unsolved, such as a small detection range, poor sensitivity, and linearity[10].

One-dimensional photonic crystals (1D-PCs) have been the focus of optoelectronics research because of their high reflection, wide bandgap, and simple structure[11–20]. In addition, the reflection and transmission spectra of 1D-PCs change with the angle of incident light. Using this interesting property, if flexible 1D-PC films can be realized, the reflection and transmission spectra will change with the curvature. In this paper, we report a curvature sensor based on flexible 1D-PC films. The curvature sensor exhibits a maximum sensitivity of 0.26 nm/m^{-1} and a wide measuring range of 33–133 m^{-1}, nearly 10 times larger than the fiber-based curvature sensors[21]. And the shift of the transmission peak varies approximately linearly with the curvature in the entire measurement range. This work provides a feasible scheme for the construction of a curvature sensor.

2. Principles and Methods

2.1. Principle of 1D-PC films curvature sensor

The structure diagram of 1D-PC is shown in Fig. 1(a), which consists of periodic low-refractive index (n_L) materials and high-refractive index (n_H) materials alternately stacked. When the number of cycles gradually increases, the photonic bandgap will gradually form in the reflection spectrum, and the larger the

number of cycles, the more obvious the photonic bandgap will be, as shown in Fig. 1(b). If a defect layer is introduced into the periodic structure, generally doubling the thickness of the intermediate layer, a defect peak will be introduced into the photonic bandgap[22,23]. One of the important characteristics of 1D-PC films is that their spectrum changes with the incident angle. Regarding Fig. 1(c), it presents the transmission spectrum of a defective 1D-PC film with a simulated central wavelength of 1500 nm. This film consists of 5 periods, and the low refractive index layer has a thickness of 246 nm, while the high refractive index layer measures 168 nm. As the angle of light increases gradually, its transmission peak gradually blue shifts, and the peak gradually decreases.

In addition, the spectra of 1D-PC films with different periodic thicknesses vary in different amplitudes with angles. Figure 1(d) shows the variation of the transmission spectrum of the defect

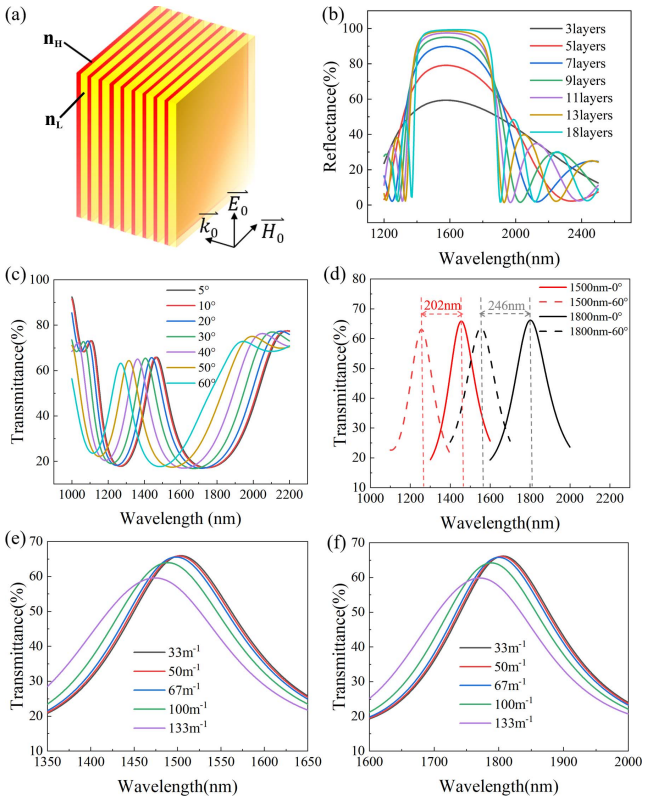

Fig. 1. Spectrum simulation of 1D-PC film. (a) Schematic diagram of 1D-PC film. (b) Simulation reflectance under different periodic layers of 1D-PC film. (c) Simulation transmittance under different incidence angles of 1D-PC film with a defect layer. The transmission peak is at 1500 nm when light is normal incidence. (d) Simulation transmittance under different periodic thicknesses of defective 1D-PC film and the shifts of transmission peaks from 0° to 60°. The two transmission peaks are at 1500 nm (red line) and 1800 nm (black line) when light is normal incidence, respectively. (e) Simulation of the variation of the transmission spectrum of defective 1D-PC film with curvature. The transmission peak is at 1500 nm when light is normal incidence. (f) Simulation of the variation of the transmission spectrum of defective 1D-PC film with curvature. The transmission peak is at 1800 nm when light is normal incidence.

1D-PC films with the center wavelength of 1500 nm and 1800 nm as the incident angle changes. As for the defect 1D-PC thin film with a simulated central wavelength of 1800 nm, it comprises 5 periods and possesses a low refractive index layer with a thickness of 296 nm, along with a high refractive index layer that is 202 nm thick. When the incident angle changes from 0° to 60°, the transmission peak of the defective 1D-PC films with a central wavelength of 1500 nm is shifted by 202 nm, while the transmission peak of the defective 1D-PC films with a central wavelength of 1800 nm is shifted by 246 nm. The larger the periodic thickness is, the larger the offset is. These properties make curvature sensors based on flexible 1D-PC films possible. Assuming that the bending radius of the circular 1D-PC film is r, its transmission spectrum can be written as

$$T = \int_0^x \frac{T_x}{S} \sqrt{2rx - x^2}\,\mathrm{d}x, \tag{1}$$

where T_x is the transmission spectrum at x, x is the position of 1D-PC film, and S is the total area of the 1D-PC film. The above calculation formula can be interpreted as follows: the total transmission spectrum of the curved 1D-PC film is the integral of the spectra of each small area with different angles. Since the curvature change will lead to the change of the included angle between each film and the incident light, the total transmission spectrum will inevitably change so that the curvature sensing can be realized.

The transmission spectrum of a 1D-PC film with different bending radii can be calculated by using Eq. (1). Figure 1(e) shows the change of transmission peak of defective 1D-PC films with a central wavelength of 1500 nm with the bending radius. As the curvature increases, the transmission peak gradually blue shifts. When the curvature changes from 33 m^{-1} to 133 m^{-1}, the defect peak shifts by 29 nm, and the sensitivity is 0.29 nm/m^{-1}. Due to the increase of periodic thickness, the transmission peak increases with the angular offset, so the increase of periodic thickness leads to the improvement of sensitivity of the defective one-dimensional photonic crystal curvature sensor. Figure 1(f) shows the change of transmission peak of the defective one-dimensional photonic crystal with a central wavelength of 1800 nm along with the bending radius. When the curvature changes from 33 m^{-1} to 133 m^{-1}, the defect peak shifts by 36 nm, and the sensitivity is 0.36 nm/m^{-1}. The increase of periodic thickness improves the sensitivity of the curvature sensor. Moreover, a detailed analysis of the curvature change response in the flexible 1D-PC films with different period numbers is provided in the Supplementary Material, Figs. S3 and S4.

2.2. Methods

In this paper, 1D-PC films are prepared by a spin coating method. The selected materials are $As_{30}S_{70}$ and PVA as high and low refractive index materials. As a chalcogenide glass, $As_{30}S_{70}$ has high transmittance and a refractive index in the near-infrared range. Meanwhile, PVA is a water-soluble polymer with good light transmittance [Supplementary Material,

Fig. S5(a)] and flexibility. The solvents of the two materials have no mutual influence on the materials, so $As_{30}S_{70}$ and PVA are a group of ideal materials for constructing high-performance flexible 1D-PC films. Additionally, both $As_{30}S_{70}$ and PVA exhibit low coefficients of thermal expansion (CTE), with $As_{30}S_{70}$ having a CTE of 24 ppm/°C and PVA having a CTE of 21 ppm/°C (ppm, parts per million)[24,25]. The compatibility of these materials is advantageous for their seamless integration into the fabrication process of flexible 1D-PC films. Their low CTE values further contribute to the films' thermal stability and resistance to temperature-induced deformations. At the wavelength of 1550 nm, the refractive indices of $As_{30}S_{70}$ and PVA are about 2.2 and 1.5, respectively, so the refractive index contrast of these two materials can be up to 0.7. The reflectivity simulations are conducted with different periodic layers according to the above theoretical thickness. When the thicknesses of PVA/$As_{30}S_{70}$ are 245/167 nm and 298/204 nm in the model, the transmission peaks are at 1500 nm and 1800 nm when the light is incident normally, respectively.

Based on the simulation results, we alternately fabricated $As_{30}S_{70}$ and PVA thin films to form periodic structures through spin-coating. During the preparation of $As_{30}S_{70}$ layers, when 100% n-propylamine or 100% n-butylamine (BA) is used as a solvent, nano-scale pores appear in the $As_{30}S_{70}$ films [see Supplementary Material, Fig. S6(a)], which greatly affect the stability and reflectivity of the 1D-PC films. The dissolution mechanism of $As_{30}S_{70}$ in n-propylamine, n-butylamine, and ethylenediamine (EDA) is different. In n-propylamine or n-butylamine, the dissolution of $As_{30}S_{70}$ results in the formation of alkyl ammonium arsenic sulfide (AAAS) salts, which lead to the formation of pores during spin-coating[26,27]. However, this problem does not appear when ethylenediamine is used as the solvent. Since the ethylenediamine molecule contains two N atoms, it chelates two arsenic centers[27], avoiding the formation of AAAS salts, and its dissolution mechanism is shown in Fig. 2(a). Therefore, adding a small amount of ethylenediamine as a mixed solvent to n-propylamine can effectively prevent the generation of pores. However, excessive ethylenediamine will cause poor wettability for $As_{30}S_{70}$ solution on the surface of the PVA film, affecting the film quality[28]. Here we use 95% n-propylamine and 5% ethylenediamine as the mixed solvent, effectively avoiding the generation of pores and ensuring wettability.

Moreover, the relative humidity in the environment during spin-coating also significantly impacts the quality of the films. Unstable relative humidity can lead to large differences in the thickness of the PVA films during the fabrication (see Supplementary Material, Fig. S7 and Table S3). Also, the spin-coating of the $As_{30}S_{70}$ layers should be executed at low relative humidity, or the film will absorb water and atomize. After spin-coating, the film is heated for uniform forming and drying, as shown in Figs. 2(b) and 2(c). At last, when the 1D-PC film is fabricated and dried, it can be easily peeled off from the substrate with tape to obtain a flexible 1D-PC film, as shown in Figs. 2(d) and 2(e).

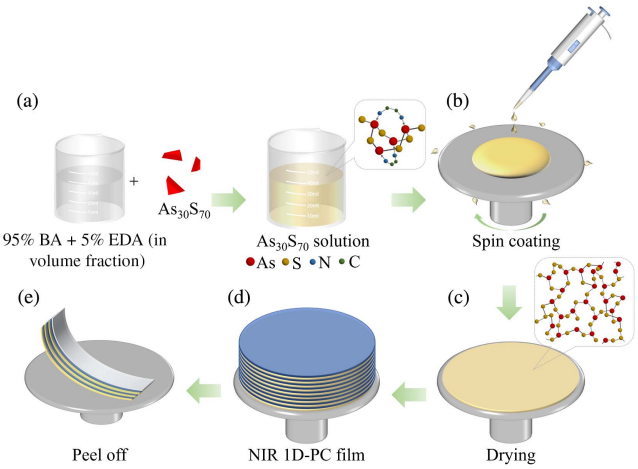

Fig. 2. The fabrication method of flexible 1D-PC film. (a) The effect of dissolving $As_{30}S_{70}$ under different solvent ratios. (b) Alternately spin-coating $As_{30}S_{70}$ solution and PVA solution while (c) drying to obtain (d) the flexible 1D-PC film. (e) Peeling off the film with tape.

3. Results and Discussion

The reflectance of the 1D-PC films gradually increases with the number of layers, as shown in Fig. 3(a), which is highly consistent with the theoretical calculation results illustrated in Fig. 1(b). It can be seen that the reflectance spectrum does not change much when the number of film layers is larger than 13 and remains essentially constant when the number of film layers is larger than 18. It is worth noting that, as the number of layers increases, the photonic bandgap's center gradually blue-shifts because the thickness of the previous spin-coated film decreases with each heating step. The scanning electron microscope (SEM) image of the cross-section of the near-infrared 1D-PC film is shown in Fig. 3(b), which clearly shows the morphology of the $As_{30}S_{70}$ and PVA films. The clear dividing line between the PVA and $As_{30}S_{70}$ indicates that there is no residual stress in each layer, and the alternate spin-coating does not affect the integrity between layers.

The comparison of transmittance, reflectance, and simulated reflectance of the 1D-PC film with 18 layers is shown in Fig. 3(c). The actual photonic bandgap reflection spectrum is consistent with the simulation results, and the photonic bandgap formed in the near-infrared band has an extremely wide bandwidth of more than 450 nm, which is more than 3 times that of all-polymer-based 1D-PC films[11,29]. Meanwhile, the experimental reflectance in Fig. 3(c) is as high as 98.1%, which is nearly 5% higher than the highest for the near-infrared flexible 1D-PC film[30]. Changing the incident angle, the near-infrared photonic bandgap reflection that is basically consistent with the simulation results (Supplementary Material, Fig. S1) can be obtained, as shown in Fig. 3(d). In order to test the repeatability of this approach, different samples were prepared under the same experimental conditions. It can be seen that the reflectance spectra of different samples are substantially identical in Fig. 3(e), which proves that the process has good repeatability (for details, see Supplementary Material, Fig. S2, Table S1, and Table S2).

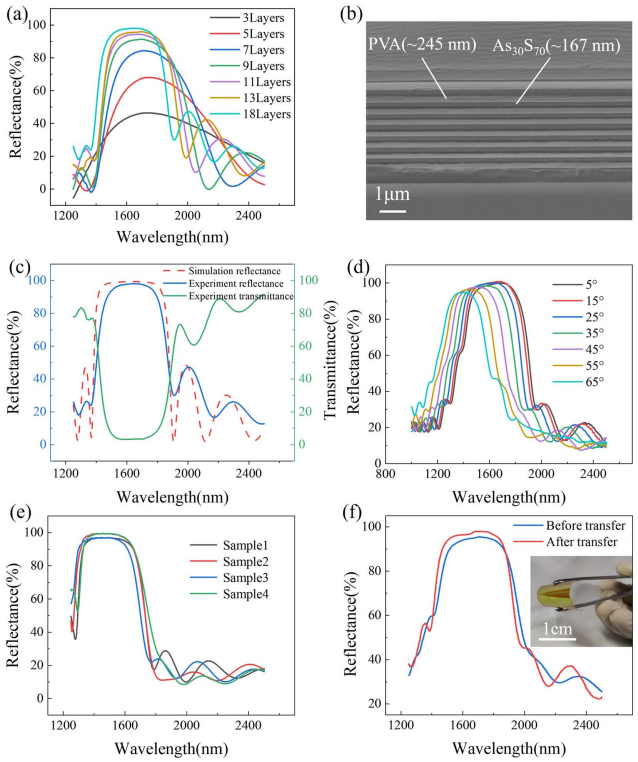

Fig. 3. Characterization of photonic bandgap spectrum of 1D-PC film prepared by spin-coating. (a) Reflectance with different periodic layers. (b) Cross-sectional SEM image of a nine-period 1D-PC film. (c) Reflection and transmission spectrum of a nine-period 1D-PC film and comparison with the simulated reflectance spectrum. (d) Reflectance under different incidence angle of 1D-PC films. (e) The reflectance spectrum of different samples is almost identical under the same parameters. (f) The comparison of the reflectance spectrum of the 1D-PC film before and after the transfer shows that there is not much difference, which proves that the film's structure is not damaged. The inset shows that the film exhibits good flexibility after transfer.

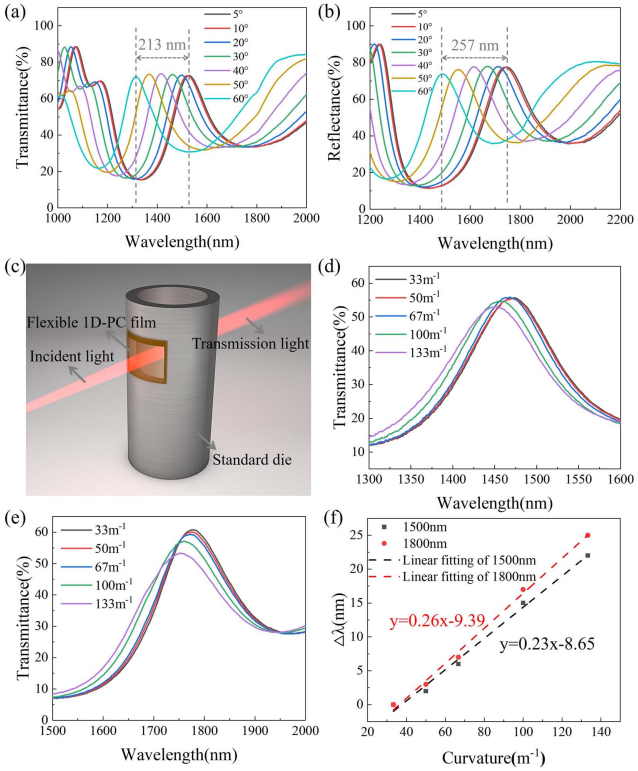

Fig. 4. Characterization of 1D-PC film curvature sensor. (a) The transmission peak of 1D-PC films with a central wavelength of 1500 nm varies with the incident angle. (b) The transmission peak of 1D-PC films with a central wavelength of 1800 nm varies with the incident angle. (c) Schematic diagram of the set-up for measuring the curvature of 1D-PC films. (d) The relationship between the central wavelength of the transmission peak and the curvature. The initial central wavelength is 1500 nm. (e) The relationship between the central wavelength of the transmission peak and the curvature. The initial central wavelength is 1800 nm. (f) Curvature response of the defective 1D-PC films with 1500 nm and 1800 nm initial peaks.

The near-infrared 1D-PC films can be easily peeled off with tape after drying, and there is almost no discrepancy between the reflectance of the films before and after the transfer, as shown in Fig. 3(f). The inset of Fig. 3(f) shows excellent mechanical properties and good flexibility of the films, potential for various flexible infrared devices. Furthermore, we placed the 1D-PC film in different ambient humidity for a while to test the effect of environmental moisture on the PVA in the film. The results show that the ambient humidity has a negligible effect on the photonic bandgap properties of the 1D-PC film, proving that the film has excellent robustness [see Supplementary Material, Fig. S5(b)]. The reason for the robustness is that the PVA thin layers in the 1D-PC film are covered by $As_{30}S_{70}$ layers, effectively preventing PVA from absorbing moisture in the environment.

By doubling the middle layer of the 1D-PC film, the defect peak can be introduced into the photonic bandgap (for details, see Supplementary Material, Fig. S8). After the experimental investigation, the total number of layers is 10, and the thickness of the fifth layer (from top to bottom, the material is PVA) is doubled. Figures 4(a) and 4(b) show the variation of the transmission spectrum of the defect 1D-PC film with the center wavelength of 1500 nm and 1800 nm, respectively, with the incident light angle. When the incident light angle increases from 5° to 60°, the transmission peaks shift by 213 nm and 257 nm, which is consistent with the above simulation calculation. And the larger the period, the larger the shift is. Figure 4(c) is a schematic diagram of measuring the transmission spectrum of defective 1D-PC film as a function of curvature. Standard dies of different diameters are used to plastic the film, thus changing the curvature of the film. Incident light is filtered through the film and into the spectrometer for analysis. It can be seen that the transmission peaks blue-shift significantly with the increasing of the films' curvature from 33 m^{-1} to 133 m^{-1} in Figs. 4(d) and 4(e). The shift of the peak position is plotted in Fig. 4(f), and a linear relationship between the shift of the peak and the film's curvature is inferred from the results. The results present that the fabricated defective 1D-PC films have a wide measuring range within 33–133 m^{-1} for curvature sensing, nearly 10 times larger than that of the fiber-based curvature sensors[21,31–33].

And the curvature sensitivities of the initial transmission peak at 1500 nm and 1800 nm are 0.23 nm/m^{-1} and 0.26 nm/m^{-1}, respectively. Obviously, the 1800-nm-curvature sensor has a higher sensitivity than the 1500-nm-curvature sensor, which is consistent with the simulation results illustrated in Figs. 1(e) and 1(f). With the same incident angle variation, the films with an initial transmission peak at 1800 nm exhibit a greater transmission peak shift than those with a transmission peak at 1500 nm, so they show a higher sensitivity to variations in the incident angle and exhibit a higher sensitivity in curvature measurement. In addition, the sensitivity of the prepared 1D-PC film curvature sensor is slightly lower than that calculated by theory, which is mainly caused by two reasons: one is that there is a certain gap between the actual period thickness and the theory, and the other is that the incident light has a divergence angle. However, this does not affect the reliability of the experimental results.

4. Conclusion

In conclusion, we propose a curvature sensor based on 1D-PC films. By taking advantage of the property of the one-dimensional photonic crystal transmission spectrum changing with the incident angle, the flexible 1D-PC films are realized for curvature sensing. High-performance near-infrared flexible 1D-PC films with a dense chalcogenide glass layer and polymer layer were fabricated by solution processing. Among them, chalcogenide glass is used as a high refractive index layer, and water-soluble polymer PVA is used as a low refractive index layer, which makes the refractive index of the two materials in 1D-PC thin films have significant differences, and the prepared 1D-PC film has good flexibility and robustness. In order to obtain a narrow transmission peak in a wide photonic bandgap, a defect layer is introduced into the periodic structure. The curvature sensitivity of 1D-PC films with initial transmission peaks at 1500 nm and 1800 nm is 0.23 nm/m^{-1} and 0.26 nm/m^{-1}, respectively. And the shift of the transmission peak varies approximately linearly with the curvature in the entire measurement range. This flexible thin-film-based curvature sensor opens up new possibilities for optical curvature sensing and measurement.

Acknowledgements

This work was supported by the National Key Research and Development Program of China (No. 2022YFB3805800), the National Natural Science Foundation of China (No. 62175082), the Science, Technology and Innovation Commission of Shenzhen Municipality (No. JCYJ20190809105615053), the Huazhong University of Science and Technology Startup Funding (No. 5003182125), and the Multidisciplinary Research Support Program of Huazhong University of Science and Technology (No. 2023JCYJ039). The authors thank the Analysis and Testing Center of HUST for the assistance with the analysis and testing.

References

1. C. Majidi, R. Kramer, and R. J. Wood, "A non-differential elastomer curvature sensor for softer-than-skin electronics," Smart Mater. Struct. **20**, 105017 (2011).
2. A. T. Asbeck, S. M. D. Rossi, I. Galiana, *et al.*, "Stronger, smarter, softer: next-generation wearable robots," IEEE Robot. Autom. Mag. **21**, 22 (2014).
3. C. K. Leung, K. T. Wan, D. Inaudi, *et al.*, "Review: optical fiber sensors for civil engineering applications," Mater. Struct. **48**, 871 (2013).
4. S. Zheng, B. Shan, M. Ghandehari, *et al.*, "Sensitivity characterization of cladding modes in long-period gratings photonic crystal fiber for structural health monitoring," Measurement **72**, 43 (2015).
5. H. Di, Y. Xin, and J. Jian, "Review of optical fiber sensors for deformation measurement," Optik **168**, 703 (2018).
6. Y. Fu, H. Di, and R. Liu, "Light intensity modulation fiber-optic sensor for curvature measurement," Opt. Laser Technol. **42**, 594 (2010).
7. M. K. Evi, D. Nikezi, and A. Djordjevich, "Monte Carlo simulation of curvature gauges by ray tracing," Meas. Sci. Technol. **15**, 1756 (2004).
8. M. S. Kovacevic, A. Djordjevich, and D. Nikezic, "Analytical optimization of optical fiber curvature gauges," IEEE Sens. J. **8**, 227 (2008).
9. Y. Fu and H. Di, "Fiber-optic curvature sensor with optimized sensitive zone," Opt. Laser Technol. **43**, 586 (2011).
10. Q. Wang and Y. Liu, "Review of optical fiber bending/curvature sensor," Measurement **130**, 161 (2018).
11. K. D. Singer, T. Kazmierczak, J. Lott, *et al.*, "Melt-processed all-polymer distributed Bragg reflector laser," Opt. Express **16**, 10358 (2008).
12. A. M. Stolyarov, L. Wei, O. Shapira, *et al.*, "Microfluidic directional emission control of an azimuthally polarized radial fibre laser," Nat. Photonics **6**, 229 (2012).
13. L. M. Goldenberg, V. Lisinetskii, and S. Schrader, "All-polymer spin-coated organic vertical-cavity surface-emitting laser with high conversion efficiency," Appl. Phys. B **120**, 271 (2015).
14. S. H. Choi, K. M. Byun, and Y. L. Kim, "Lasing interactions disclose hidden modes of necklace states in the Anderson localized regime," ACS Photonics **5**, 881 (2017).
15. T. Heuser, R. Merindol, S. Loescher, *et al.*, "Photonic devices out of equilibrium: transient memory, signal propagation, and sensing," Adv. Mater. **29**, 1606842 (2017).
16. P. Lova, G. Manfredi, and D. Comoretto, "Advances in functional solution processed planar 1D photonic crystals," Adv. Opt. Mater. **6**, 1800730 (2018).
17. A. H. Aly, S.-W. Ryu, H.-T. Hsu, *et al.*, "THz transmittance in one-dimensional superconducting nanomaterial-dielectric superlattice," Mater. Chem. Phys. **113**, 382 (2009).
18. A. H. Aly, A. A. Ameen, M. A. Mahmoud, *et al.*, "Photonic crystal enhanced by metamaterial for measuring electric permittivity in GHz range," Photonics **8**, 416 (2021).
19. A. H. Aly, S. E. S. Abdel Ghany, B. M. Kamal, *et al.*, "Theoretical studies of hybrid multifunctional $YaBa_2Cu_3O_7$ photonic crystals within visible and infra-red regions," Ceram. Int. **46**, 365 (2020).
20. A. H. Aly, S. K. Awasthi, A. M. Mohamed, *et al.*, "1D reconfigurable bistable photonic device composed of phase change material for detection of reproductive female hormones," Phys. Scr. **96**, 12 (2021).
21. G. Salceda-Delgado, A. Van Newkirk, J. E. Antonio-Lopez, *et al.*, "Compact fiber-optic curvature sensor based on super-mode interference in a seven-core fiber," Opt. Lett. **40**, 1468 (2015).
22. A. H. Aly and D. Mohamed, "The optical properties of metamaterial-superconductor photonic bandgap with/without defect layer," J. Supercond. Novel Magn. **32**, 1897 (2018).
23. A. H. Aly, S. K. Awasthi, M. A. Mohaseb, *et al.*, "MATLAB simulation-based theoretical study for detection of a wide range of pathogens using 1D defective photonic structure," Crystals **12**, 220 (2022).
24. S. J. Skuban, F. Skuban, S. R. Lukiæ, *et al.*, "Thermal coefficient of linear expansion of non-crystalline chalcogenides in the As-S-Se-Te-I system," J. Therm. Anal. Calorim. **71**, 439 (2003).
25. K. Wei, X. Xiao, W. Xu, *et al.*, "Large programmable coefficient of thermal expansion in additively manufactured bi-material mechanical metamaterial," Virtual Phys. Prototyp. **16**, S53 (2021).
26. G. C. Chern and I. Lauks, "Spin-coated amorphous chalcogenide films," J. Appl. Phys. **53**, 6979 (1982).
27. T. A. Guiton and C. G. Pantano, "Solution/gelation of arsenic trisulfide in amine solvents," Chem. Mater. **1**, 558 (1989).

28. Y. Zha, S. Fingerman, S. J. Cantrell, *et al.*, "Pore formation and removal in solution-processed amorphous arsenic sulfide films," J. Non-Cryst. Solids **369**, 11 (2013).
29. T. Kazmierczak, H. Song, A. Hiltner, *et al.*, "Polymeric one-dimensional photonic crystals by continuous coextrusion," Macromol. Rapid Commun. **28**, 2210 (2007).
30. T. S. Kleine, L. R. Diaz, K. M. Konopka, *et al.*, "One dimensional photonic crystals using ultrahigh refractive index chalcogenide hybrid inorganic/organic polymers," ACS Macro Lett. **7**, 875 (2018).
31. B. Dong, J. Hao, and Z. Xu, "Temperature insensitive curvature measurement with a core-offset polarization maintaining photonic crystal fiber based interferometer," Opt. Fiber Technol. **17**, 233 (2011).
32. Z. Ou, Y. Yu, P. Yan, *et al.*, "Ambient refractive index-independent bending vector sensor based on seven-core photonic crystal fiber using lateral offset splicing," Opt. Express **21**, 23812 (2013).
33. L. Mao, P. Lu, Z. Lao, *et al.*, "Highly sensitive curvature sensor based on single-mode fiber using core-offset splicing," Opt. Laser Technol. **57**, 39 (2014).